Optics Letters

Large thermal tuning of a polymer-embedded silicon nitride nanobeam cavity

Yueyang Chen,[1] (iD) James Whitehead,[1] Albert Ryou,[1] Jiajiu Zheng,[1] (iD) Peipeng Xu,[1,3,4] (iD) Taylor Fryett,[1] and Arka Majumdar[1,2,*] (iD)

[1]Electrical and Computer Engineering, University of Washington, Seattle, Washington 98195, USA
[2]Department of Physics, University of Washington, Seattle, Washington 98195, USA
[3]Laboratory of Infrared Materials and Devices, Advanced Technology Research Institute, Ningbo University, Ningbo 315211, China
[4]Key Laboratory of Photoelectric Detection Materials and Devices of Zhejiang Province, Ningbo 315211, China
*Corresponding author: arka@uw.edu

Tunable silicon nitride nanophotonic resonators are a critical building block for integrated photonic systems in the visible wavelength range. We experimentally demonstrate a thermally tunable polymer-embedded silicon nitride nanobeam cavity with a tuning efficiency of 44 pm/°C and 0.13 nm/mW in the near-visible wavelength range. The large tuning efficiency comes from the high thermo-optic coefficient of the SU-8 polymer and the "air-mode" cavity design, where a large portion of the cavity field is confined inside the polymer region. The demonstrated resonator will enable locally tunable cavity quantum electrodynamic experiments in the silicon nitride platform. © 2019 Optical Society of America

Integrated silicon photonic devices, taking advantage of their compact size and scalable fabrication technology, have recently experienced an outpouring of diverse applications, ranging from optical communication, quantum information science, and biomedical sensing in the infrared (IR) to mid-IR wavelength range [1–5]. For extending the photonic platform to the visible wavelength range while maintaining the compatibility with silicon-based fabrication, silicon nitride (SiN) becomes an attractive choice of material because of its broad transparent window and low scattering loss [6–8]. Various SiN photonic devices including on-chip spectrometers [9], large-scale phased arrays [10], and hybrid light sources [11] have been demonstrated in the visible wavelength range. Unfortunately, efficient tuning of SiN devices remains difficult: as a centro-symmetric material with a large bandgap, SiN has a low thermo-optic coefficient ($\sim 10^{-5}/°C$) and lacks both free-carrier dispersion and second-order nonlinearity. Tunability is critical for advanced applications, such as bringing resonators to the same frequency [12,13], creating a reconfigurable switching network [14], or dynamic phased array.

In this Letter, we experimentally demonstrate an SU-8 polymer-embedded SiN nanobeam cavity with a high tuning efficiency of 44 pm/°C and 0.13 nm/mW in the near-visible wavelength range. The key to this high tunability is the large thermo-optic (TO) coefficient ($\sim 10^{-4}/°C$) of the polymer [15]. The SU-8 polymer is chosen because of the high TO coefficient [16,17], ultralow absorption in the near-visible wavelength range [18], and its compatibility with the photonic crystal structures as shown previously [16,17]. The ease of spin-coating SU-8 on a SiN substrate also makes the integration process straightforward, and several experiments have already demonstrated such integration [19].

The schematic of the device is shown in Fig. 1. The SiN nanobeam sits on a silicon oxide substrate, with the SU-8 polymer cladding and filling the patterned holes. The polymer-SiN nanobeam cavity is designed to have an "air mode" [20–23], in which a large portion of the electromagnetic field is confined inside the low-index material, which, in our case, is the polymer. A gold heater is fabricated next to the patterned holes; driving a current heats up the polymer and subsequently tunes the cavity resonance.

We first design the polymer-SiN air-mode nanobeam cavity. Due to the relatively low refractive index contrast of SiN ($n = 2$) to SU-8 polymer ($n = 1.574$) and silicon dioxide ($n = 1.45$), it is nontrivial to design a high-Q photonic crystal cavity on this platform [24]. Compared to the traditional suspended SiN nanobeam cavity, our on-substrate nanobeam cavity also increases the mechanical robustness of the cavity
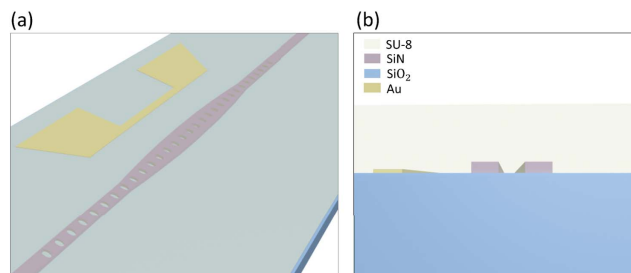

Fig. 1. Schematic of the polymer-embedded SiN resonator, with an electrical heater placed nearby.

and eliminates the risk of the structure breaking during fabrication. In our design, the SiN unit cell has a Bragg period $a = 225$ nm and a width of $w = 500$ nm, comprising an elliptical hole with the long axis equal to 290 nm and the short axis equal to 116 nm. A SU-8 cladding layer filling the holes with a thickness of 500 nm is incorporated in the band structure calculation, performed via MIT photonics bands (MPBs) [25] [Fig. 2(a)]. There are two bands below the light cone. We focus on the upper band (shown in red), known as the "air band," where a large portion of the electromagnetic field is distributed inside the SU-8 regime, as shown in the cross-section diagram in Fig. 2(b).

We then define the high-Q air mode by tapering the waveguide width from the Bragg region (500 nm) to the center (699 nm) following the relation: $w(x) = w_{center} + x^2(w_{end} - w_{center})/x_{max}^2$ [16], where x increases from zero (at the center of the nanobeam) to the end of the taper region. The number of periods in the Bragg region (taper region) is 20 (30), with the period fixed at 225 nm. Figure 2(c) shows the cavity-mode profile calculated via finite-difference time-domain method (FDTD) simulation. The cavity has anti-nodes inside the holes, which are filled by the polymer. The cavity mode has a wavelength of ~730 nm with a Q-factor of ~10^5. The mode volume of the cavity is calculated as ~$20\left(\frac{\lambda}{n_{su-8}}\right)^3$. We note that the mode volume is larger than that of a traditional

photonic crystal cavity, but is still significantly smaller than other on-chip SiN resonators, such as micro-disk or micro-ring resonators [7,8].

We simulate the TO tuning of the device using FDTD method. The tuning of the effective mode index of the nanobeam cavity can be expressed in the first order as

$$\frac{dn_{eff}}{dT}(\lambda) = \Gamma_{SiN}(\lambda)\frac{dn_{SiN}}{dT}(\lambda) + \Gamma_{SU-8}(\lambda)\frac{dn_{su-8}}{dT}(\lambda),$$

where $\frac{dn_{eff}}{dT}$ is the effective TO coefficient, and $\Gamma_{SiN}(\lambda)$ and $\Gamma_{Su-8}(\lambda)$ represent the confinement factor of the cavity field inside the SiN and the SU-8 polymer region, respectively. We calculate the confinement factor (defined as $\frac{\int_{region}\varepsilon E^2 dV}{\int_{mode}\varepsilon E^2 dV}$) in SU-8, SiN, and silicon oxide as 47%, 41%, and 12%, respectively, from the cavity-mode profile via FDTD simulation. From numerical simulation, we also find that a higher effective TO coefficient ($\frac{dn_{eff}}{dT}$) might be achieved if a thermal-optic polymer with higher refractive index is used, since it would result in a larger confinement factor inside the polymer region. $\frac{dn_{SiN}}{dT}$ and $\frac{dn_{SU-8}}{dT}$ are the TO coefficient of SiN (~2.45×10^{-5}/°C [26]) and SU-8 polymer, respectively. The TO coefficient of uncured SU-8 is documented in the range from -1.8×10^{-4}/°C to -3.5×10^{-4}/°C [16,17], depending on the condition of fabrication.

Since the electromagnetic field possesses the highest confinement factor in the polymer region and SU-8 has a much higher (and negative) TO coefficient compared to SiN, we expect to observe a blue shift of the cavity resonance when we apply heat. As shown in Fig. 2(d), the cavity blue shifts by 6 nm (2.9 nm) across a 100°C temperature increase, when the TO coefficient of the SU-8 is assumed as -3.5×10^{-4}/°C (-1.8×10^{-4}/°C), corresponding to a tuning efficiency of 60 pm/°C (29 pm/°C). On the other hand, a bare SiN cavity with a dielectric mode is tuned by 0.9 nm across a 100°C temperature increase, corresponding to a tuning efficiency of only 9 pm/°C. We also simulate an electrical heater using finite element method to identify the optimum distance of the heater from the cavity. A close proximity will give rise to strong absorptive losses from the metal, whereas if the heater is placed too far away, the cavity will not be heated. From the simulations, we find a good tradeoff when the heater is 1.5 μm away from the nanobeam structure. As shown in Fig. 2(e), when the heater temperature is 250°C, the temperature at the nanobeam reaches 100°C.

We then experimentally validate our theory. We fabricated the cavity using a 220-nm-thick SiN membrane grown via LPCVD on 4 μm of thermal oxide on silicon. The samples were obtained from commercial vendor Rogue Valley Microelectronics. We spun roughly 400 nm of Zeon ZEP520A, which was coated with a thin layer of Pt/Au that served as a charging layer. The resist was then patterned using a JEOL JBX6300FX electron-beam lithography system with an accelerating voltage of 100 kV. The pattern was transferred to the SiN using a reactive ion etch (RIE) etch in CHF_3/O_2 chemistry. The heating electrode with 500-nm width and 20-μm length was defined via electron-beam overlay and evaporation followed by a lift-off process. Figure 3(a) shows a scanning electron micrograph (SEM) of the fabricated SiN cavities on thermal oxide just after etching. Grating couplers are fabricated on both sides of the nanocavity for the transmission
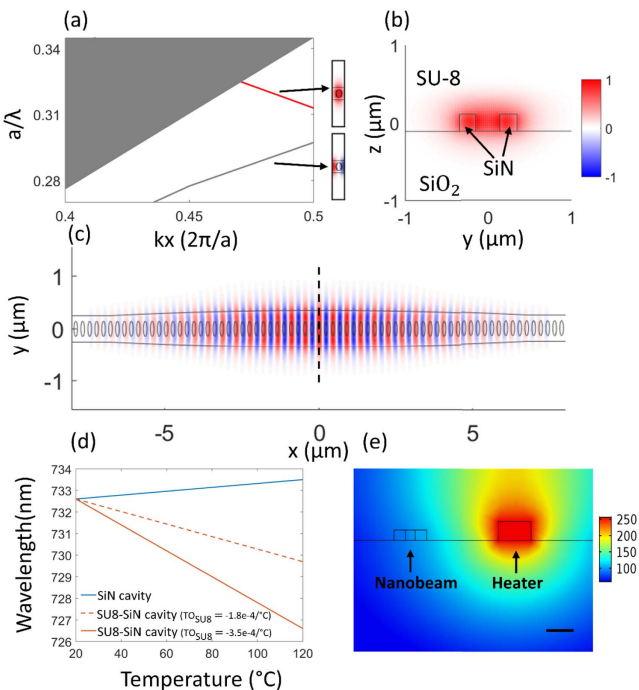

Fig. 2. Device design: (a) band structure of the unit cell. (b) Electric field distribution of the wave-guide cross section for the air band. (c) FDTD simulation of the cavity field distribution. (d) Comparison of the simulated tuning efficiency of a bare silicon nitride nanobeam cavity and the SU8-SiN nanobeam cavity. The blue line shows the tuning of a bare SiN cavity. The red dashed line shows the tuning of a SU-8-SiN cavity assuming the TO coefficient of SU-8 as -1.8×10^{-4}/°C. The red solid line shows the tuning of the SU-8-SiN cavity assuming the TO coefficient of SU-8 as -3.5×10^{-4}/°C. (e) Thermal simulation shows that the side heater can efficiently heat up the cavity region. Scale bar: 500 nm.
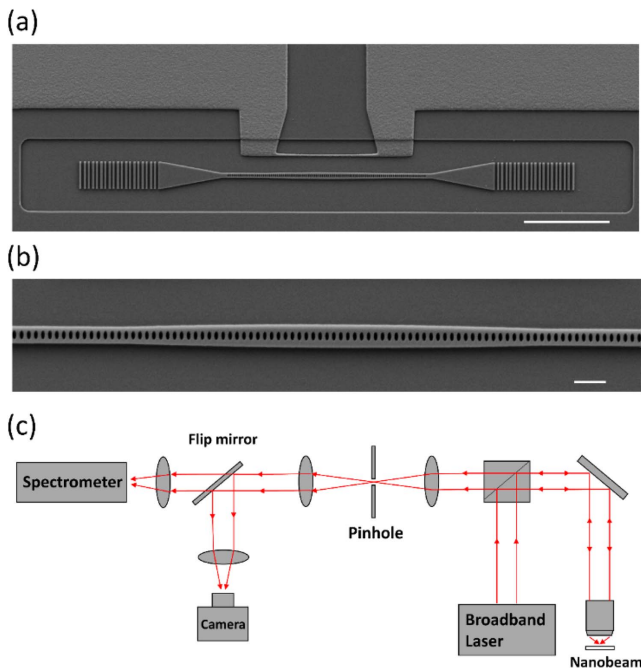
(a)

(b)

(c)

Fig. 3. (a) SEM image of the device shows the nanobeam cavity, grating couplers, and metal heater. Scale bar: 10 μm. (b) Zoom-in image of the nanobeam: the width of the nanobeam waveguide is parabolically tapered to achieve a high Q-factor air mode. Scale bar: 1 μm. (c) Confocal microscopy setup for the transmission measurement of the nanobeam cavity.

measurement. Figure 3(b) shows the parabolic tapering of the width of the nanobeam waveguide to confine the mode in the air. After the device was fabricated, we spun coated SU-8 on top of the cavity. We used SU-8-2000.5 from microChem because of its small viscosity needed to fill the holes. A similar experiment with a silicon photonic crystal cavity has been reported before showing that the holes can be filled with SU-8 [16]. After the spin coating, we baked the chip at 95°C for 1 min to further remove the solvent.

The cavities are characterized via measuring the transmission using a confocal microscopy setup [Fig. 3(b)]. A super continuum light source (Fianium WhiteLase Micro) is focused on the grating coupler through the objective lens, and a moveable pinhole is used to pick up only the signal coming out from the other grating and then send it to a spectrometer. The spectrometer is equipped with a Princeton Instruments PIXIS CCD with an IsoPlane SCT-320 Imaging Spectrograph. The cavity at room temperature has a Q-factor ~6500 and resonance wavelength at 731 nm. The smaller Q-factor compared to our simulation result is attributed to fabrication imperfections due to small feature sizes at near-visible wavelength operation.

We first characterized the thermal tuning by heating up the whole chip in a hot plate. As shown in Fig. 4(a), between 20°C and 70°C, we tuned the cavity from 731.3 nm to 728.9 nm, corresponding to a tuning efficiency of 44 pm/°C. We fit the TO coefficient of the SU-8 by the experimentally achieved tuning efficiency in FDTD simulation and extracted the value to be -2.5×10^{-4}/°C, which lies in the range of the documented values [16,17]. Then we used the electrical heater to tune the cavity, as shown in Fig. 4(b). By applying 12.5 mW power
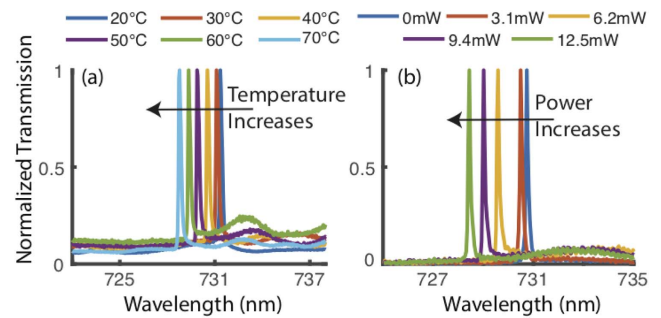

Fig. 4. (a) Hot plate tuning: the cavity is tuned from 731.3 nm to 728.9 nm by a temperature rise of 50°C, corresponding to a tuning efficiency of 44 pm/°C, matching well with the theory. (b) Electrical heating: by applying 12.5 mW power to the side heater, the resonance is tuned by 1.625 nm, corresponding to a tuning efficiency of 0.13 nm/mW.

to the side heater, we tuned the resonance by 1.625 nm, corresponding to a tuning efficiency of 0.13 nm/mW. We applied a train of square pulses (power_high = 9.4 mW, power_low = 6.2 mW, period = 1 s, duty cycle = 30%) to the metal heater in a continuous 3-h experiment, while the nanobeam cavity was irradiated by a super-continuum laser source for the cavity transmission measurement. We observed a consistent tuning of the cavity resonance between 729.6 nm and 729 nm on the spectrometer, which confirmed that the thermal tuning of the polymer-SiN cavity was reversible and robust. We did not observe any degradation of our device 56 days after fabrication, which was confirmed by the consistent cavity quality factor in our measurement.

To further analyze the thermal tuning performance of our device, we adapted the Lumped Element Circuit Model of the TO devices [27]. For a thermal-tunable optical resonator, the TO detuning corresponding to π phase shift is derived as [21]

$$\Delta\lambda = \frac{\pi\lambda_0}{Q},$$

where λ_0 is the cavity resonance wavelength and Q is the quality factor. For our device, the power required for π phase shift is calculated as

$$P_\pi = \frac{\Delta\lambda}{0.13 \text{ nm/mW}} = \frac{\pi \times 730 \text{ nm}}{0.13 \text{ nm/mW} \times 6500} = 2.7 \text{ mW}.$$

We compared the tuning energy efficiency (nm/mW) and P_π with other thermally tunable SiN nano-photonic devices (Table 1) and found that our device had the highest tuning efficiency and lowest P_π.

In conclusion, we experimentally demonstrate a thermally tunable polymer-embedded SiN nanobeam cavity with a tuning efficiency of 44 pm/°C and 0.13 nm/mW in the

Table 1. Tuning Performance for Various SiN Nanophotonic Devices

Device	Energy (nm/mW)	Power P_π (mW)
SiN ring [29]	8.2×10^{-4}	7.7
SiN MZI [30]	NA	30
SU-8-SiN cavity (this work)	0.13	2.7

near-visible wavelength range. The large tuning efficiency comes from the high TO coefficient of the SU-8 polymer and our air-mode cavity design, where a large portion of cavity field is confined inside the polymer. Further higher TO polymer can be used such as polyurethane (PUR) [28]. Our tunable cavity can potentially have applications in the development of reconfigurable optical devices and cavity quantum electrodynamics experiments on the SiN platform.

REFERENCES

1. D. A. B. Miller, Proc. IEEE **97**, 1166 (2009).
2. J. Wang, S. Paesani, Y. Ding, R. Santagati, P. Skrzypczyk, A. Salavrakos, J. Tura, R. Augusiak, L. Mančinska, D. Bacco, D. Bonneau, J. W. Silverstone, Q. Gong, A. Acín, K. Rottwitt, L. K. Oxenløwe, J. L. O'Brien, A. Laing, and M. G. Thompson, Science **360**, 285 (2018).
3. X. Qiang, X. Zhou, J. Wang, C. M. Wilkes, T. Loke, S. O'Gara, L. Kling, G. D. Marshall, R. Santagati, T. C. Ralph, J. B. Wang, J. L. O'Brien, M. G. Thompson, and J. C. F. Matthews, Nat. Photonics **12**, 534 (2018).
4. M. Iqbal, M. A. Gleeson, B. Spaugh, F. Tybor, W. G. Gunn, M. Hochberg, T. Baehr-Jones, R. C. Bailey, and L. C. Gunn, IEEE J. Sel. Top. Quantum Electron. **16**, 654 (2010).
5. R. Soref, Nat. Photonics **4**, 495 (2010).
6. J. F. Bauters, M. J. R. Heck, D. John, D. Dai, M.-C. Tien, J. S. Barton, A. Leinse, R. G. Heideman, D. J. Blumenthal, and J. E. Bowers, Opt. Express **19**, 3163 (2011).
7. A. Gondarenko, J. S. Levy, and M. Lipson, Opt. Express **17**, 11366 (2009).
8. E. S. Hosseini, S. Yegnanarayanan, A. H. Atabaki, M. Soltani, and A. Adibi, Opt. Express **17**, 14543 (2009).
9. B. Momeni, E. S. Hosseini, and A. Adibi, Opt. Express **17**, 17060 (2009).
10. C. V. Poulton, M. J. Byrd, M. Raval, Z. Su, N. Li, E. Timurdogan, D. Coolbaugh, D. Vermeulen, and M. R. Watts, Opt. Lett. **42**, 21 (2017).
11. Y. Chen, A. Ryou, M. R. Friedfeld, T. Fryett, J. Whitehead, B. M. Cossairt, and A. Majumdar, Nano Lett. **18**, 6404 (2018).
12. A. W. Elshaari, E. Büyüközer, I. E. Zadeh, T. Lettner, P. Zhao, E. Schöll, S. Gyger, M. E. Reimer, D. Dalacu, P. J. Poole, K. D. Jöns, and V. Zwiller, Nano Lett. **18**, 7969 (2018).
13. T. Fan, Z. Xia, A. Adibi, and A. A. Eftekhar, Opt. Lett. **43**, 4887 (2018).
14. A. H. Atabaki, A. A. Eftekhar, S. Yegnanarayanan, and A. Adibi, Opt. Express **21**, 15706 (2013).
15. Z. Zhang and N. Keil, Opt. Commun. **362**, 101 (2016).
16. Y. Zhang and Y. Shi, Opt. Lett. **40**, 264 (2015).
17. Y. Zhang, P. Liu, S. Zhang, W. Liu, J. Chen, and Y. Shi, Opt. Express **24**, 23037 (2016).
18. M. T. Do, T. T. N. Nguyen, Q. Li, H. Benisty, I. Ledoux-Rak, and N. D. Lai, Opt. Express **21**, 20964 (2013).
19. Z. Zhang, D. Liu, D. de Felipe, A. Liu, N. Keil, and N. Grote, Appl. Phys. Lett. **102**, 181105 (2013).
20. R. Miura, S. Imamura, R. Ohta, A. Ishii, X. Liu, T. Shimada, S. Iwamoto, Y. Arakawa, and Y. K. Kato, Nat. Commun. **5**, 5580 (2014).
21. Q. Quan and M. Loncar, Opt. Express **19**, 18529 (2011).
22. D. Yang, H. Tian, and Y. Ji, Appl. Opt. **54**, 1 (2015).
23. B.-H. Ahn, J.-H. Kang, M.-K. Kim, J.-H. Song, B. Min, K.-S. Kim, and Y.-H. Lee, Opt. Express **18**, 5654 (2010).
24. T. K. Fryett, Y. Chen, J. Whitehead, Z. M. Peycke, X. Xu, and A. Majumdar, ACS Photon. **5**, 2176 (2018).
25. S. G. Johnson and J. D. Joannopoulos, Opt. Express **8**, 173 (2001).
26. A. Arbabi and L. L. Goddard, Opt. Lett. **38**, 3878 (2013).
27. H. Lin, Y. Song, Y. Huang, D. Kita, S. Deckoff-Jones, K. Wang, L. Li, J. Li, H. Zheng, Z. Luo, H. Wang, S. Novak, A. Yadav, C.-C. Huang, R.-J. Shiue, D. Englund, T. Gu, D. Hewak, K. Richardson, J. Kong, and J. Hu, Nat. Photonics **11**, 798 (2017).
28. G. Coppola, L. Sirleto, I. Rendina, and M. Iodice, Opt. Eng. **50**, 071112 (2011).
29. X. Xue, Y. Xuan, C. Wang, P.-H. Wang, Y. Liu, B. Niu, D. E. Leaird, M. Qi, and A. M. Weiner, Opt. Express **24**, 687 (2016).
30. A. Mohanty, Q. Li, M. A. Tadayon, G. Bhatt, E. Shim, X. Ji, J. Cardenas, S. A. Miller, A. Kepecs, and M. Lipson, "A reconfigurable nanophotonics platform for sub-millisecond, deep brain neural stimulation," arxiv:1805.11663 (2018).